Finite element model and validation of a surrogate crash test vehicle for impacts with roadside objects

Azim Eskandarian, Dhafer Marzougui, and Nabih E. Bedewi
FHWA/NHTSA National Crash Analysis Center, The George Washington University
20101 Academic Way, Ashburn, Virginia 20147

(Received 30 September 1996; and in revised form 10 May 1997)

Abstract - Highway and roadside safety features are crash tested for compliance with certain safety criteria. US Federal Highway Administration (FHWA) uses a surrogate reusable test vehicle, Bogie, to conduct crash tests of roadside safety features. Bogie is intended to replace an impacting vehicle in order to reduce the cost of the test. Bogie can be configured with different crushable impact noses representing various vehicle fronts. Typically, the crushable nose employed by Bogie is a multi-compartment honeycomb material. Different configurations of honeycomb arrangement are considered for different impact velocities. Recently, the advances in crashworthiness and dynamic finite element analysis have allowed considerable modelling and simulation of vehicle impacts with roadside hardware. This paper describes, in detail, the finite element models and the validation of Bogie and its honeycomb material in impacts with an instrumented rigid pole. This model can be exercised in various simulations of crash scenarios for design optimization of roadside hardware. This validation also allows the use of the model for impacts with narrow objects, which is a critical aspect of crashes with roadside safety devices.

NOTATION

ρ Density
ν Possion's ratio
E Elastic or Young's modulus
G Elastic shear modulus
μ Material viscosity coefficient
σ_y Yield stress for fully compacted honeycomb material
τ Shear stress
V Relative volume, the ratio of the current volume over the initial volume of honeycomb
V_f Relative volume at which the honeycomb is fully compacted
a,b,c Subscripts defining the honeycomb cell depth, ribbon, and transverse direction, respectively
i,j Subscript index for a,b, and c directions
u Subscript designating uncompacted honeycomb
β Coefficient for calculation of E_{ii} and G_{ij}
E_{aau}, E_{bbu}, E_{ccu} Three elastic moduli of honeycomb in uncompressed configuration
G_{abu}, G_{bcu}, G_{cau} Three elastic shear moduli of honeycomb in uncompressed configuration
max (value1, value2) Function returns the maximum of two values
min (value1, value2) Function returns the minimum of two values
σ_{aa}, σ_{bb}, σ_{cc}, σ_{ab}, σ_{bc}, and σ_{ca} Stress components

INTRODUCTION

Roadside safety appurtenances, e.g., guard rails, bridge rails, median barriers, and roadside hardware (sign supports, luminare poles, etc.) are designed to redirect the vehicles, reduce the vehicle speed, or break upon impact. These safety features are intended to reduce the occupant injuries in vehicle crashes with roadside devices. The performance of the roadside safety appurtenances traditionally is evaluated by full-scale crash tests. These devices are continuously undergoing design changes and being improved upon for safety compliance. The changes are made based on the evaluation of the field performance and the resulting accident/injury statistics.

US Federal Highway Administration (FHWA) and the State Departments of Transportation play a major role in the development of safety criteria and the testing of the roadside appurtenances.

The crash testing of roadside devices using vehicles is a very costly undertaking. The variety of devices to be tested, the different classes of vehicles for which safety compliance must be checked, and the number of various impact conditions that need to be evaluated require an extensive matrix of crash tests to be conducted. This is definitely a prohibitive cost requirement. Therefore, improvements in the design of many roadside safety features are only incremental due to the lack of comprehensive test data and performance measures.

The vehicle is a major cost element in the crash testing of roadside appurtenances. In many cases, the reusable surrogate test vehicle, Bogie, is used in lieu of the impacting vehicles to reduce the test cost. The use of Bogie also expedites the test setup and preparation because the acquisition, instrumentation, and preparation of new vehicles usually requires a longer lead time and often delays the test schedule. Bogie, on the other hand, is equipped with all the necessary instrumentation and can be easily reconfigured with various impact noses to represent different vehicle frontal crush characteristics. Many tests for the performance evaluation of roadside safety features are therefore conducted with Bogie.

Advances in crashworthiness research [1-4] and particularly in dynamic finite element analysis of impacts [5-10] has opened up new possibilities for the evaluation of the crash performance of roadside appurtenances. In recent years, non-linear explicit finite element codes have significantly advanced the computer modelling and simulation of automobile crashes [11-20]. This capability additionally allows the application of the software to model and analyse the performance of roadside objects in crashes [21-24]. The simulations can assist the redesign and optimization of these devices for the purpose of reducing injuries in highway accidents. The codes used are based on various public domain and commercial versions of the DYNA3D program[25-27]. The authors have been applying these codes in various highway safety analysis projects [10-13, 21-23], in particular, in addressing collisions with highway narrow objects like sign support systems. At present, many models of roadside safety features are being developed by various researchers using DYNA3D software in a coordinated FHWA program. The unavailability of functional, computationally efficient and validated, impacting vehicle models is a major impediment to these roadside hardware crash simulation efforts. Since most of the tests are conducted using Bogie, the need for a validated model for the bogie is evident.

To this end, a DYNA3D model of the FHWA's Bogie has been developed. The model incorporates a multi-compartment crushable honeycomb nose. The experimental testing and the process for validation of the individual honeycomb segments as well as for the validation of the entire vehicle model in impacts with an instrumented rigid pole is described. The validation with the rigid pole, as opposed to the rigid wall, is of special interest because it is a better measure of performance of the honeycomb in impacts with highway narrow objects, because roadside narrow objects (poles, signs, etc.) are a major cause of severe injury in highway crashes [28]. Much testing is conducted by FHWA to evaluate the performance of these objects in crashes.

FHWA crash tests the roadside appurtenances to discover shortcomings in the existing or proposed designs, and to assure compliance with the requirements of the NCHRP (National Highway Cooperative Research Program) Report 350 [29]. In the NCHRP 350 test criteria, various roadside hardware must be evaluated in crashes with various classes of vehicles including

the Small Size Vehicle denoted by 700C and 820C representing 700 and 820 kg vehicle weights, respectively. Certain devices are allowed to be tested using surrogate vehicles like Bogie. For this application, Bogie simulates the small or light weight vehicle class.

The goal of this research is to arrive at a validated DYNA3D finite element model of Bogie that can be used (1) initially as a predictor for the crash tests and (2) eventually as a tool for design parametric studies to optimize the performance of the roadside safety appurtenances in reducing the crash pulse intensity in highway collisions.

FHWA SURROGATE TEST VEHICLE, BOGIE

The Federal Highway Administration's (FHWA) Bogie is a surrogate vehicle used for the full scale crash test of highway appurtenances [30-31]. Bogie is used in crash tests by FHWA to simulate the impact dynamics of a small size vehicle. It can be configured with different noses to represent different crush characteristics. Each frontal nose represents a different class of vehicle or impactor [32]. Its weight can also be slightly adjusted with ballast to represent weight variations within a vehicle class category. Bogie used here, shown in Figure 1, simulates NCHRP's 820C vehicle.

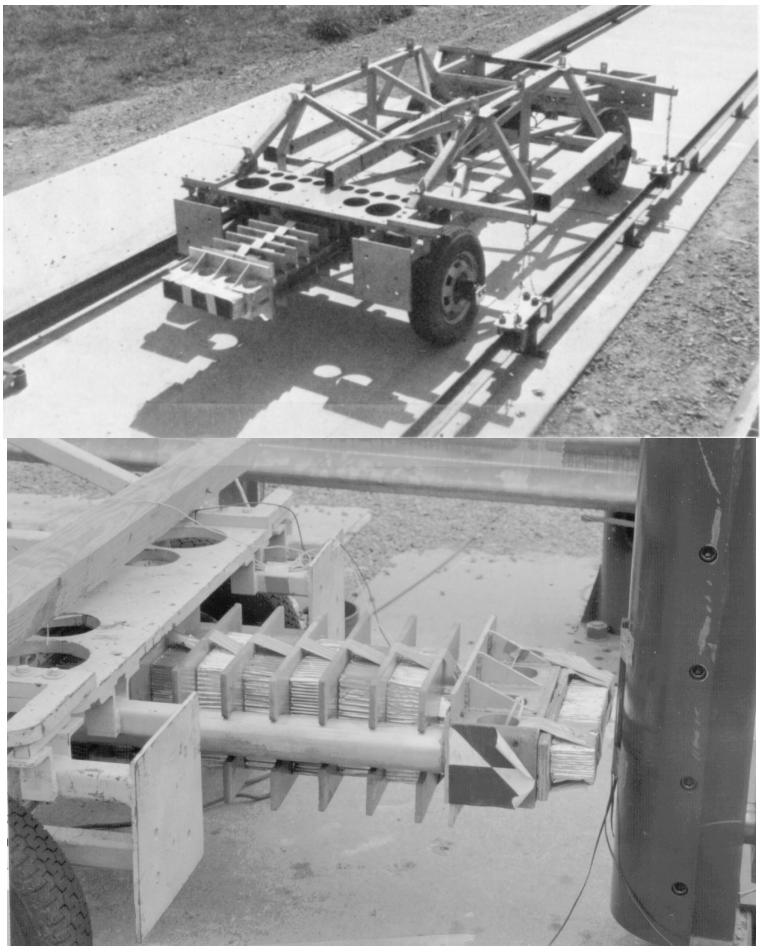

Figure 1. Bogie- surrogate crash test vehicle

Bogie is basically an un-powered four-wheeled rigid structure which is guided and accelerated with an external drive mechanism, e.g., a weight pulley system or a towing winch system, to

arrive at a desired impact angle and velocity. Bogie is equipped with an accelerometer at the approximate location of the C.G.. The accelerometer is contained in an instrument box which is connected to the off-board data acquisition system via an umbilical cord. The rigidity of Bogie's structure behind the nose assuages concerns about the accuracy of acceleration measurement and simplifies some of the complexities of the FE modeling.

In impact tests of roadside hardware, two noses are widely used: 1) a rigid nose, and 2) a flexible honeycomb nose. The rigid nose model does not truly require a validation since both the structure and the impactor are rigid and practically act as a rigid body with the specified weight and inertia distribution. Figure 2 is a schematic drawing showing the dimensions of Bogie. The flexible honeycomb nose consists of multiple compartments of honeycomb material, possibly of different consistencies, i.e., different crushability. The compartments are separated by 12.7 mm (0.5 in) fiberglass plates. The nose assembly is attached to two shafts which are guided to slide through Bogie's front structure (two structural tubes). This arrangement allows the plates and honeycomb segments to be compacted consecutively upon impact as the whole assembly slides through Bogie's rigid structure. A fore bumper (frontal block) honeycomb segment is also attached to reduce the initial impact spike. Figure 3 shows the sketch of the honeycomb nose.

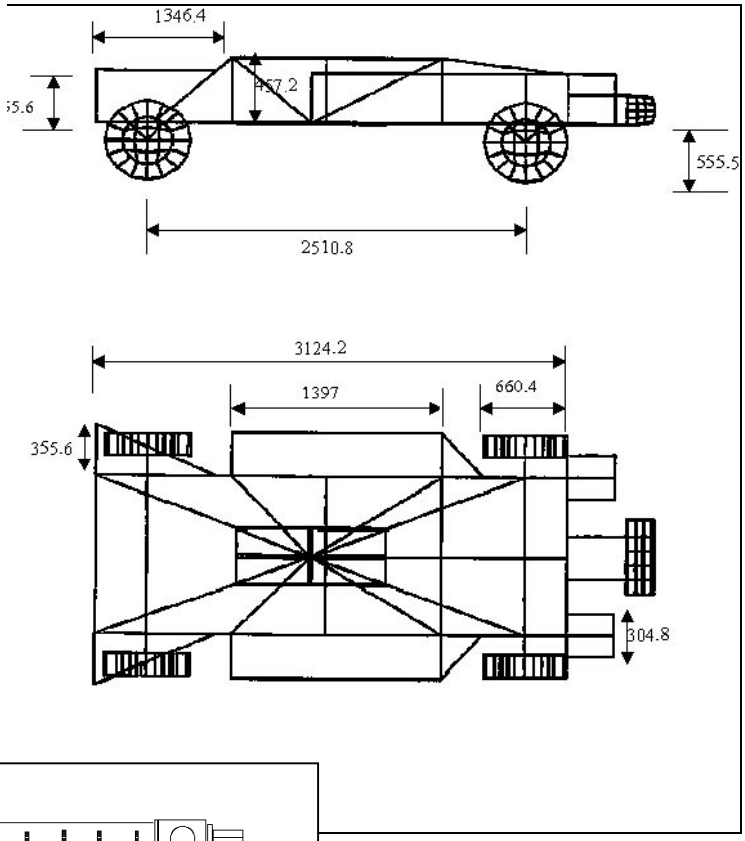

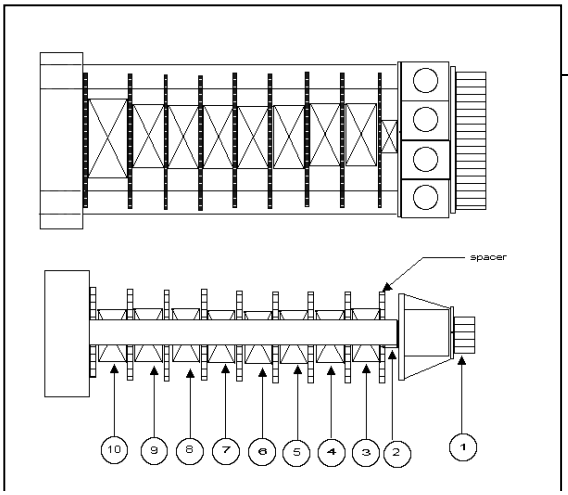

Figure 2. Dimensions of Bogie

Cartridge #	Size in (mm)	Type	Static Crush Strength (KPa)
1	70x406x76	HC130	896
2	102x127x51	HC025	172
3	203x203x76	HC230	1585
4	203x203x76	HC230	1585
5	203x203x76	HC230	1585
6	203x203x76	HC230	1585
7	203x203x76	HC400	2756
8	203x203x76	HC400	2756
9	203x203x76	HC400	2756
10	203x254x76	HC400	2756

Figure 3. Configuration of the honeycomb impacting nose

FINITE ELEMENT MODEL

All models in this paper are developed using MSC/PATRAN and LS-INGRID pre-processors. The LS-DYNA3D program is the solver. The post-processing is done using LS-TAURUS.

Bogie structure

A LS-DYNA3D model of Bogie's structure is developed. The vehicle structure is appropriately modeled with beam, shell, and solid elements where applicable. Since for all practical purposes Bogie has a rigid structure, the application of various type of elements has insignificant effect on the performance of the model. However, special attention is paid to assure geometrical accuracy, weight distribution and inertial properties. Material properties and the model description for Bogie are summarized in Table 1. Figure 4 shows the finite element model of Bogie with the installed honeycomb nose.

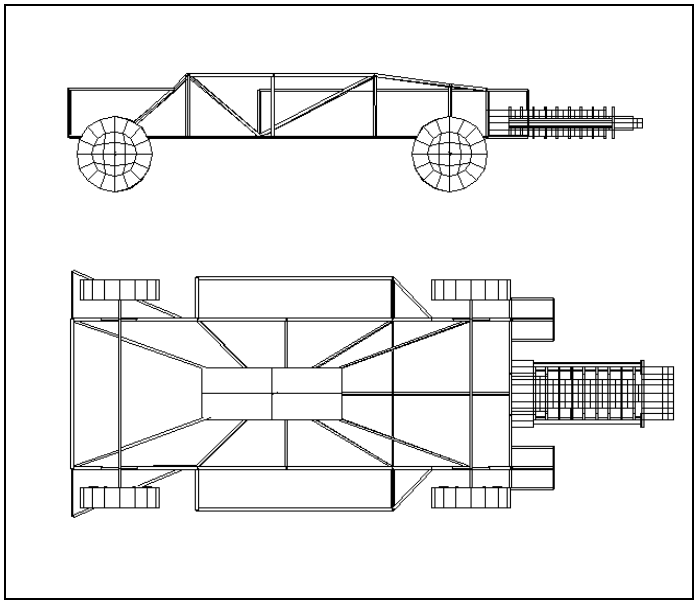

Figure 4. Finite element model of Bogie

Table 1. Bogie material properties and finite element model description

Type and Number of Elements	**Parts**	**Young's modulus** MPa	**Possion's ratio**	**Density** kg/mm^3	**Yield Stress** MPa
Beam (126)	Structural beams	20.0×10^4	0.30	0.785×10^{-5}	207.0
Shell (384)	Steel Plates	20.0×10^4	0.30	0.785×10^{-5}	207.0
	Steel Hub	20.0×10^4	0.30	0.785×10^{-5}	207.0
	Rubber tire	2.4615×10^3	0.323	0.106×10^{-5}	24.77
Solid (1286)	Instruments Box	1.25×10^4	0.33	0.785×10^{-5}	207.0

Testing and validation of honeycomb material model

The flexible nose modelled here is one of many flexible honeycomb configurations available for crash tests. The nose that was originally designed for 32 km/hr (20 mph) impacts, representing a 1979 VW Rabbit, is modeled. The crash test data of this configuration impacting an instrumented rigid pole is used for validation of the nose model. This configuration consists of ten compartments (segments) of four different honeycomb consistencies separated by fiberglass plates. The honeycomb segments are designated by FHWA as type number 25, 130, 230, and 400 based on their manufacturer listed crush strength. Segment model 130 acts as fore-bumper to reduce the initial spike of the impacts and is supported by a 27.2 kg block. The remaining honeycomb assembly comprises one honeycomb 25, four honeycomb segments 230 and four honeycomb segments 400, totaling ten honeycomb segments. These are attached to the rear end of the impact bumper block. These segments are arranged in groups separated by retaining plates as shown in Figure 3.

Material model

A LS-DYNA3D model of the multi-layer honeycomb nose was developed to represent the crush characteristics and stiffness of the actual honeycomb configuration. This model was developed in multiple steps. Each honeycomb segment has its own stiffness and crush characteristics that need to be modelled and verified separately in DYNA3D. LS-DYNA3D metallic honeycomb material model type 26 was used. This material model requires multiple parameters that describe the properties of each honeycomb segment. These parameters are listed in Table 2.

Having four different designs in ten compartments, there are four times as many parameters needed than the number required for modeling the entire nose in DYNA3D. Therefore, the evaluation and verification of the entire model at once, without characterization of the individual segments, is almost an impossible exercise. Although the crush characteristic of the entire

Honeycomb Nose impactor is available from crash test data, the characteristics of the individual segments still need to be determined.

Table 2. LS-DYNA3D (Material Type 26) parameters for the metallic honeycomb material

Parameter	Description
ρ	Density
E	Young's modulus for honeycomb material
ν	Possion's ratio for honeycomb material
σ_y	Yield stress for fully compacted honeycomb material
Load curves	Load curve for σ_{aa} , σ_{bb}, σ_{cc} , σ_{ab} , σ_{bc}, and σ_{ca} and τ versus either relative volume or volumetric strain (default: load curves for b and c are equal to the one for direction aa). Each component of shear stress may have its own load curve (default: load curves for shear are equal to the one for direction aa).
Load curves	Optional load curve for strain rate effects
V_f	Relative volume at which the honeycomb is fully compacted
E_{aau}, E_{bbu}, E_{ccu}	Three elastic moduli in uncompressed configuration
G_{abu}, G_{bcu}, G_{cau}	Three elastic shear moduli in uncompressed configuration
μ	Material viscosity coefficient. (default=0.5)
Failure point	Tensile strain at element failure (element will erode)
Failure point	Shear strain at element failure (element will erode)

In LS-DYNA3D [25] the behavior of the honeycomb before compaction is orthotropic where the components of the stress tensor are uncoupled (i.e., a component of the strain will generate resistance in the local a-direction with no coupling to the other two local directions.) The elastic moduli vary from their initial values to the fully compacted values linearly with the relative volume:

$$E_{ii} = E_{iiu} + \beta(E - E_{iiu}) \quad , \qquad \text{ii= aa, bb, and cc} \qquad (1)$$

$$G_{ij} = G_{iju} + \beta(G - G_{iju}) \quad , \qquad \text{ij= ab, bc, and ca} \qquad (2)$$

where aa is the axial (direction of impact) or the honeycomb cell depth direction, bb and cc are the honeycomb ribbon and transverse directions respectively, and

$$\beta = \max\left[\min\left(\frac{1-V}{1-V_f}, 1\right), 0\right] \qquad (3)$$

where G is the elastic shear modulus for the fully compacted honeycomb material found from

$$G = \frac{E}{2(1+\nu)} \quad . \qquad (4)$$

The relative volume, V, is defined as the ratio of the current volume over the initial volume and typically, V=1 at the beginning of a calculation. V_f designates the relative volume at full compaction. As shown above, accurate determination of E_{iiu} and V_f has a major effect on the modelling of the honeycomb properties.

In the computation of stresses, as volumetric compaction occurs, the directional elastic moduli vary linearly from their initial values to the fully compacted value according to equations 1 and 2. In partially compacted states, the stress components are limited by the maximum values at the current relative volume V as specified on the load curves [26]. For fully compacted material, the assumption is that material behavior becomes elastic- perfectly plastic.

The appendix provides a glossary of the honeycomb material properties and testing configurations as defined by the manufacturer [33]. The directions aa, bb, and cc defined in LS-DYNA3D material type 26 correspond to thickness or cell depth, i.e., impact direction, longitudinal or ribbon direction, and transverse direction, respectively.

The material parameters, including load curves for each honeycomb segment, are defined as follows:

Properties and load curves

The mechanical properties, Young's modulus, Poisson's ratio, yield stress, density, and the elastic shear modulus of 5052 Military Grade Alloy Aluminum Honeycomb are used. For fully compacted material the properties of the Aluminum Alloy are used and the honeycomb characteristics are taken from the manufacturer's data.

Load curves define the magnitude of the average stress as the material changes density. In order to construct the load curves, samples of each honeycomb segment were quasi-statically compression tested in a series of laboratory experiments using an MTS testing machine. From these tests, load deflection curves were derived. Using the load-deflection data, the engineering stress-strain curves are generated. The slope of the stress-strain curve in the elastic region defines the value for the elastic modulus in the uncompressed configuration, E_{aau}. The manufacturer's data on the elastic moduli were verified by this technique. Also, the relative volume at full compaction, V_f, can be determined from this curve by observing the point of sudden change in the slope where the force consistently increases with minimal or no increase in displacement or volume. The compression tests provide the axial deflections (displacements). The cross-section of the test specimen is known; hence, the volume can be approximated using the product of the displacement and the cross-sectional area. The G_{iju} value for verification of the manufacturer's data can be obtained from equation (4).

Other parameters and assumptions

Additional assumptions were made to define completely all necessary LS-DYNA3D parameters for material type 26 shown in table 2. The lateral deformation and changes in the non-axial (axial direction is aa) orthogonal directions, namely directions bb and cc, are neglected. Therefore, the default load curves were used for these directions. The justification is that in our application, the honeycomb segments are free to expand laterally and have no contact forces and reactions in these directions and in the LS-DYNA3D treatment of the uncompacted honeycomb, the components of the stress tensor are uncoupled as described in the above material model. There is no coupling between the generated strain in the local aa direction and the bb and cc directions.

The failure model option was not exercised. Basically the material was assumed to compress under load until full compaction and to continue to resist the load with no failure, which is typically observed in this application of the honeycomb material.

The material viscosity option was not exercised as recommended by the LS-DYNA3D manual. This assumption mitigates any concerns in interpreting the force data as described by Schwer and Whirley [34], when a coefficient of bulk viscosity resulted in a pork barrel effect where there was an interface between the honeycomb and the containing plate members. Schwer and Whirley, using the fundamental physics of the problem, justified a DYNA3D shortcoming in computation of axial forces when there is an interface between a honeycomb and its retaining plate. They attributed this effect to the coefficient of bulk viscosity, and show that decreasing the value of this parameter empirically will alleviate the problem. This factor has not been shown to have any effect in our honeycomb assembly configuration.

Experiments and validation of honeycomb properties

Compression tests were conducted quasi-statically to characterize the parameters of each honeycomb segment separately. Each compression test is duplicated with an individual LS-DYNA3D model to insure the correct material behavior for each segment in simulation. The force versus crush response (load-deflection curves) of compression tests and simulations are compared in Figures 5 to 8. The results show a very close agreement between simulation and test data, proving the accuracy of the specified material properties. The same load curve properties are used in the fully-assembled nose model.

Table 3 lists the honeycomb properties and the data extracted from the four load curves used for the four different honeycomb materials.

Table 3. Properties of four honeycomb segments

Property	**Honeycomb 25**	**Honeycomb 130**	**Honeycomb 230**	**Honeycomb 400**
E (MPa)	0.68950×10^5	0.68950×10^5	0.68950×10^5	0.68950×10^5
G (MPa)	0.25921×10^5	0.25921×10^5	0.25921×10^5	0.25921×10^5
ν	0.33	0.33	0.33	0.33
σ_y (MPa)	0.220683×10^3	0.220683×10^3	0.220683×10^3	0.220683×10^3
ρ (tons/mm^3)	0.16018×10^{-10}	0.49657×10^{-10}	0.68880×10^{-10}	0.91305×10^{-10}
V_f	0.120	0.200	0.220	0.240
E_{aau}, E_{bbu}, E_{ccu} (MPa)	0.68950×10^2	0.51711×10^2	0.96527×10^2	0.15168×10^2
G_{abu} (MPa)	0.48263×10^2	0.15168×10^2	0.20822×10^2	0.27579×10^2
G_{bcu} (MPa)	0.89630×10^2	0.28820×10^2	0.42058×10^2	0.57916×10^2
G_{cau} (MPa)	0.48263×10^2	0.15168×10^2	0.20822×10^2	0.27579×10^2

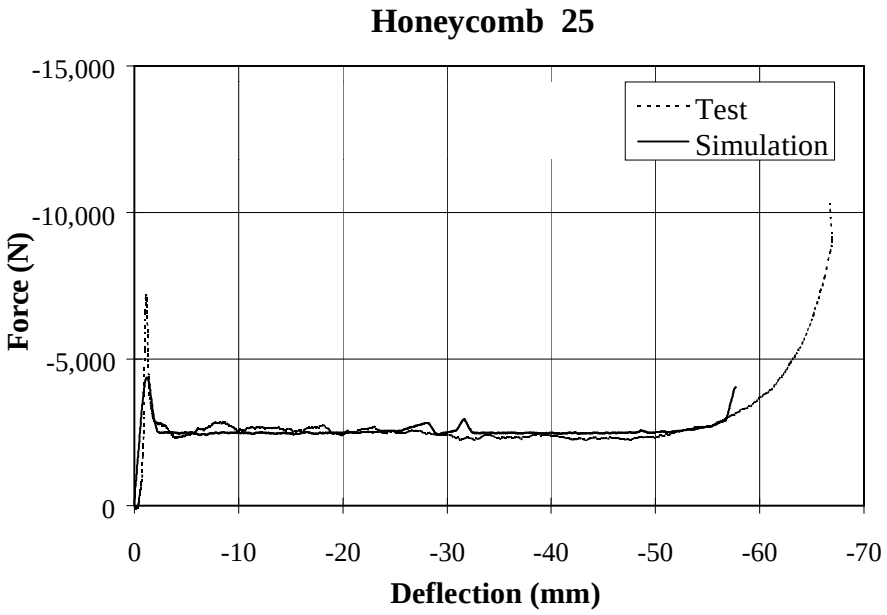

Figure 5. Comparison of compression test and simulation of honeycomb 25 material.

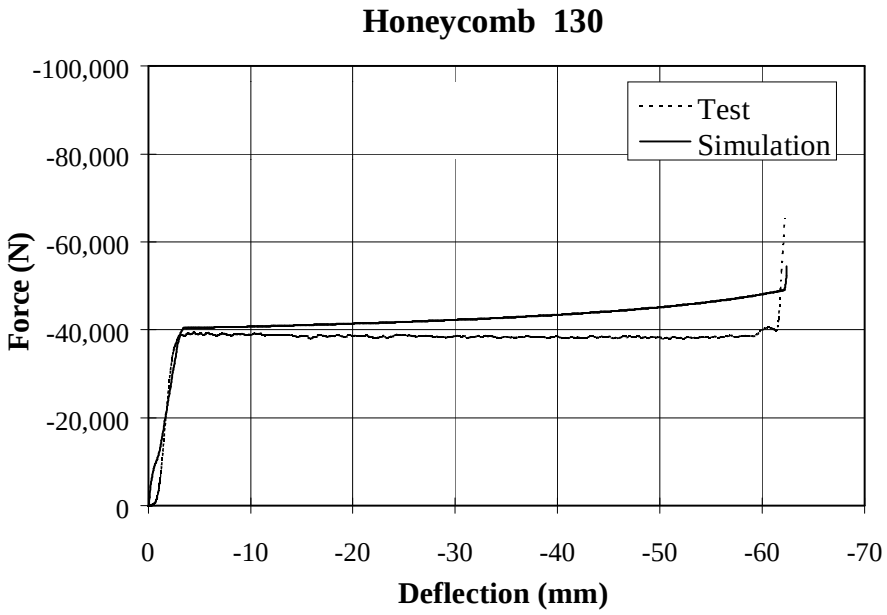

Figure 6. Comparison of compression test and simulation of honeycomb 130 material.

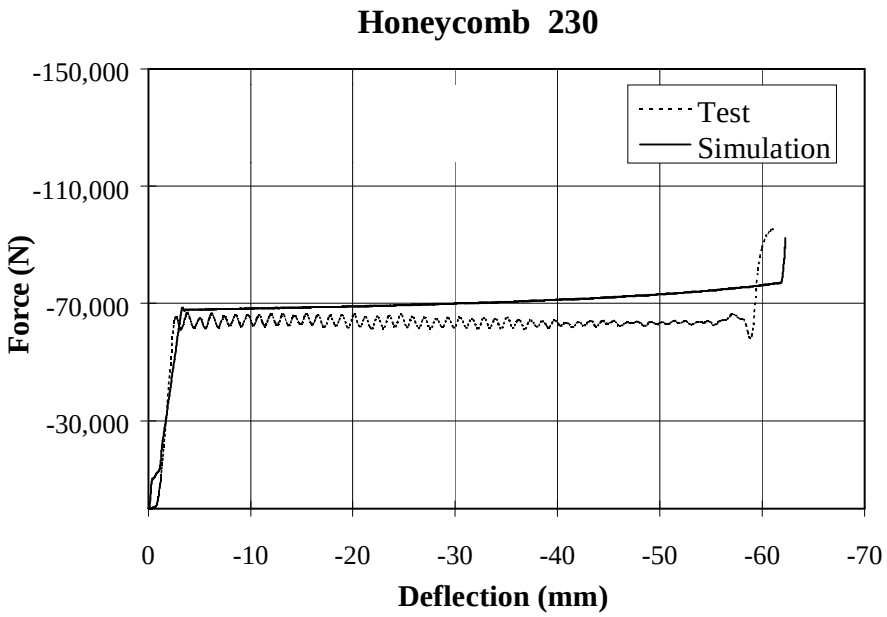

Figure 7. Comparison of compression test and simulation of honeycomb 230 material.

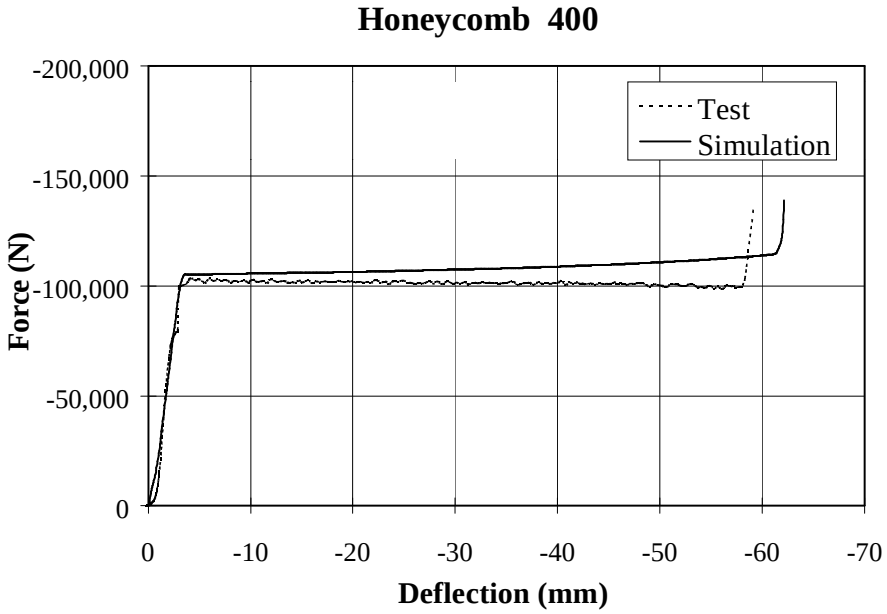

Figure 8. Comparison of compression test and simulation of honeycomb 400 material.

BOGIE VALIDATION RESULTS AND DISCUSSIONS

After each segment was modelled satisfactorily, a model of the entire honeycomb assembly (nose) was developed and compared with the calibration test results. The material properties are specified according to the data verified by the individual simulations and compression tests. The nose is attached to Bogie. One of the crash tests conducted at the FHWA's FOIL (Federal Outdoor Impact Laboratory) is simulated [35]. In this exercise, Bogie (800 kg) with honeycomb nose impacts a 219 mm (8 5/8 in) diameter rigid pole at 32 km/h (20 mph). Figure 9 shows the consecutive crush time history of the crash simulation. The zoomed-in plot highlights the impression of the pole cross section in the bumper and reflects the successive crush of the individual honeycomb segments between retaining plates as the impact progresses. There are three main stages of crush corresponding to the three different aft-bumper block honeycomb types, namely, type 25, 230, and 400.

Figure 10 shows the simulated deformation (crush) is almost identical to the actual crash test result. The states at which the crush are compared correspond to the successive stages that each honeycomb type (multiple segments for each type) undergoes until maximum compaction. These states can also be observed in the acceleration plots described below. For example, the first stage from zero to 15 ms of the crash reflects the crushing of the honeycomb type 130 (fore-bumper block) and type 25 (aft-bumper block). The pictures are captioned from the high-speed crash test film. Only a few states are captured from the film due to the fact that a major part of the crush is invisible under Bogie's flat plate. The simulation acceleration is compared with the accelerometer measurements from the crash test. The accelerometer is placed approximately at Bogie's C.G. in an instrument box. The acceleration is computed and velocity and displacements are found by integrating the acceleration time history. The comparison of the test and simulation time histories of acceleration, velocity and displacement are shown in Figures 11 to 13, respectively.

The velocity and displacement plots reveal an excellent agreement between the model response and the crash test data. The acceleration, although capturing the general response of the pulse, shows minor local deviations. A major contributor to the initial pulse discrepancies is the low stiffness characteristics of the honeycomb segment 25 as shown in Figure 5. The load curve used for this material is the one generated from figure 5, which shows an initially stiffer simulated model than the actual compression tested material. This exact characteristic is clearly reflected in the assembled nose model (Figures 9, 10 and 11). Since this segment is the first one to absorb the bumper block energy in the impact, it has a major effect in shaping the few initial pulses. This effect is observed in the acceleration time history plot (Figure 11). Another cause of discrepancies may be the difference between the dynamic and static compression (compaction) properties of the individual honeycomb segments which are not evaluated in this study. The manufacturer estimates a difference of possibly as much as 30% in mechanical properties obtained from static and dynamic compression tests.

The simulated nose of Bogie is only considered for the low speed impacts (approximately 32 to 48 km/hr). There are no crash test data available for the validation of the nose at higher speeds. Higher speed crash tests with rigid poles are intentionally avoided because of the risk of damaging Bogie. Higher speed impact tests for collapsible poles and other roadside hardware are available, but can not be used for validation because they raise the issue of the validity of the model of the impacted object itself.

In addition, we can not overlook the sensitivities of the honeycomb material itself, as well as the approximations resulting from our modelling assumptions, e.g., the lateral and shear forces are

ignored and no provision is made for the sliding friction forces between the honeycomb segments and their respective retaining plates, all of which may contribute to energy absorption and the change in the initial axial pulse.

In summary, after examining the general trend of the acceleration pulse and the correlation of the resulting velocity-time histories, we can consider this model to be validated for low speed impacts with roadside objects. The model is also suitable for narrow object impacts. Roadside objects are typically evaluated by their capability to redirect the vehicle or reduce the impact speed. Neither dummies nor any other direct measure of the occupant injury is utilized in the evaluation process. Therefore, models that can duplicate or provide the information that is normally provided by a roadside hardware test will still be of significant value. Without falsely justifying the shortcomings of the existing model for precise evaluation of the initial crash pulses, the presented model possess sufficient fidelity for its intended purpose; it can indeed be used effectively to predict the outcome of impacts of Bogie with roadside devices. After all, the resulting velocity and displacement time-histories from the model very closely trace the crash test data.

Although not presented here, this Bogie model has been successfully used by the authors in simulating crashes with various highway narrow objects including a hat-cross section small sign support pole and an omni-directional slip-base sign and luminare support poles. It also continues to be used for simulating the low-speed impacts of various roadside objects like guardrails, end-terminals, etc.

CONCLUSIONS

A detailed DYNA3D FE model of FHWA's surrogate crash test vehicle is developed and validated using a 32 km/hr (20 mph) impact with an instrumented rigid pole. The surrogate test vehicle, Bogie, is used by the US Federal Highway Administration for testing the impact performance of various roadside appurtenances at low to mid-range speeds. Bogie is equipped with a multi-compartment impactor "nose" assembly made of aluminum honeycomb material. The validation included a laboratory experimentation and comparison with FE models of four different honeycomb segments as well as the parameter identification and impact performance evaluation of the entire nose assembly with crash test data. The results show the model can indeed provide reliable results and be used for the evaluation of impact performance of the roadside appurtenances.

This model can be used by the investigators that are currently focusing on modelling the roadside hardware. This tool results in significant cost reduction by reducing the number of crash tests required for a comprehensive evaluation of many roadside appurtenances, especially for the evaluation of impacts with narrow objects which statistics indicate to be a critical cause of injury in highway crashes.

At present, high-speed crash tests of highway appurtenances are not conducted using Bogie but vehicle tests at high speeds are required by the NCHRP 350 safety criteria. Therefore, future work may focus on using the presented modelling method for the validation of honeycomb impactors designed for higher-speed crashes. Additional validation with test data for crashes at different speeds and angles and honeycomb material representing the crush characteristics of different classes of vehicles will also be very beneficial to highway crashworthiness safety research.

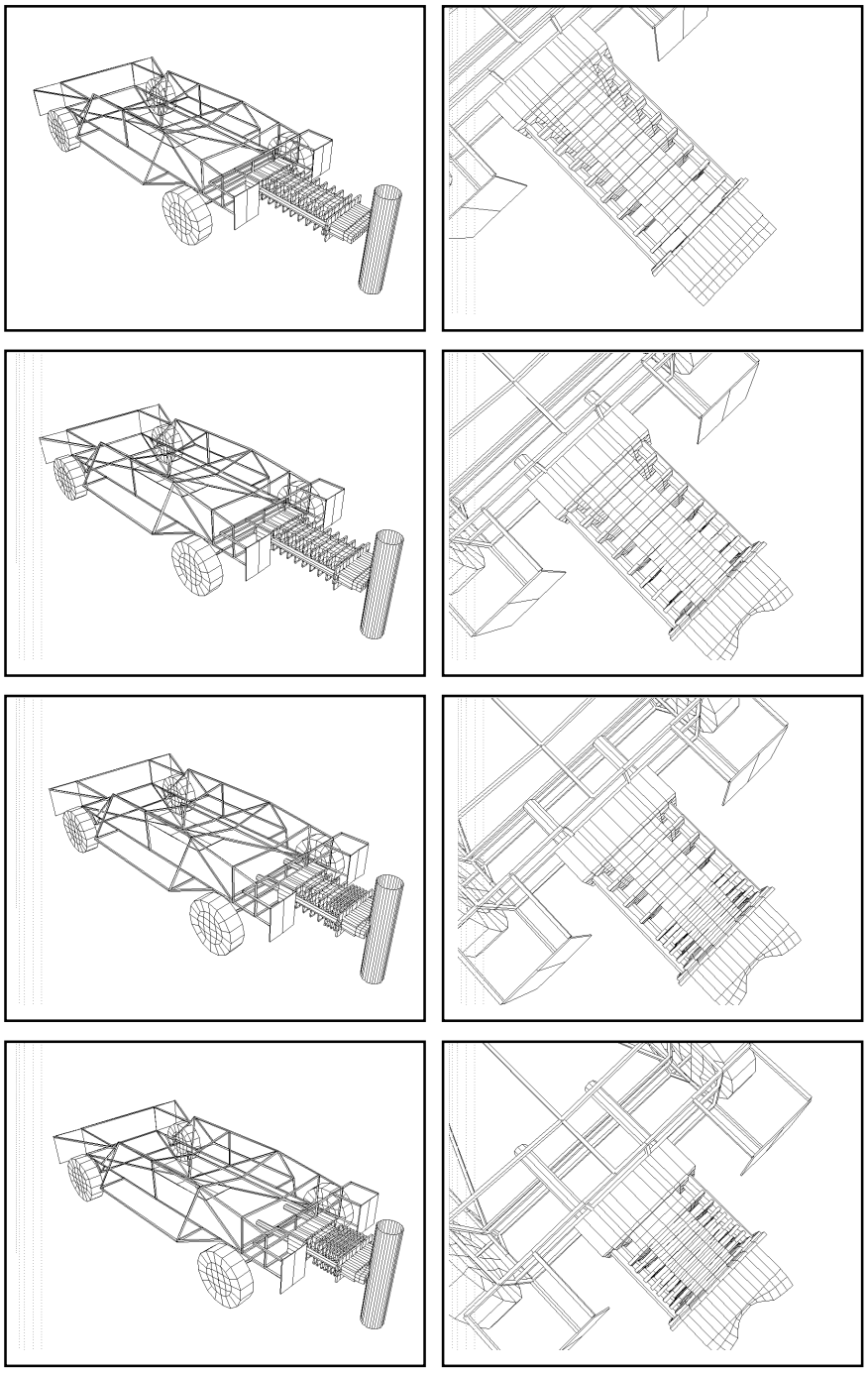

Figure 9. Initial and deformed honeycomb nose in a 32 km/hr impact with a rigid pole reflecting the successive crush of honeycomb segments

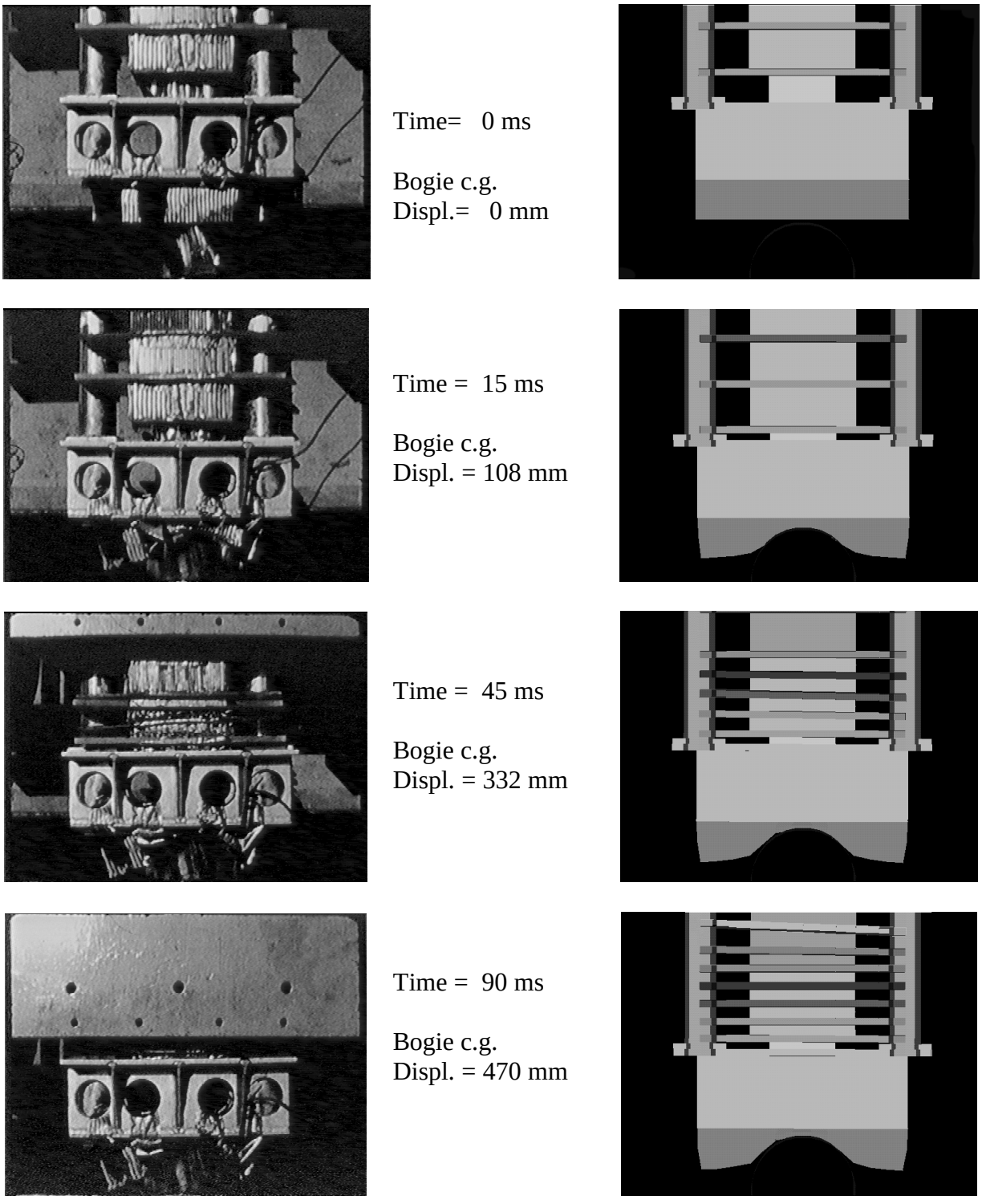

Figure 10. Comparison of simulation and crash test results showing successive crush (deformation) of the honeycomb nose material

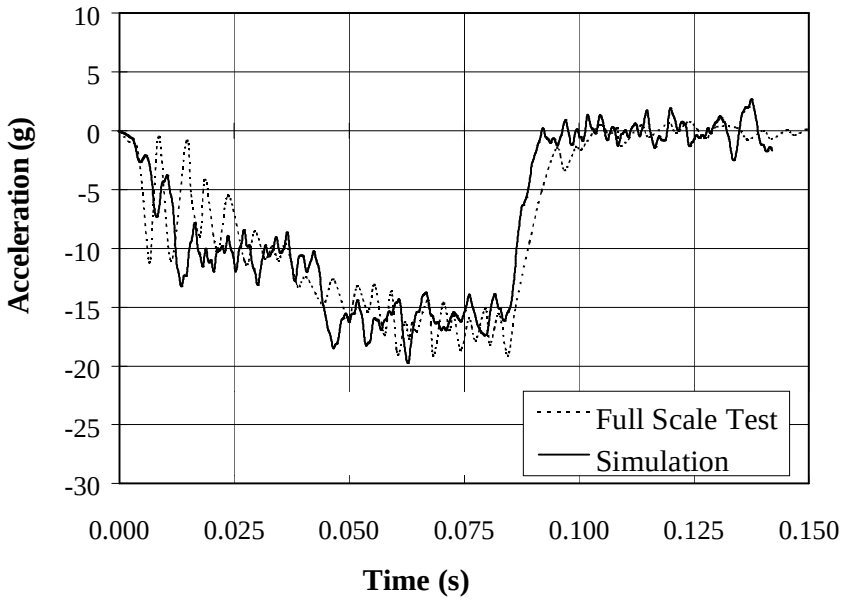

Figure 11. Comparison of acceleration time histories from crash test and simulation of Bogie impacting a rigid pole at 32 km/hr. (20 mph)

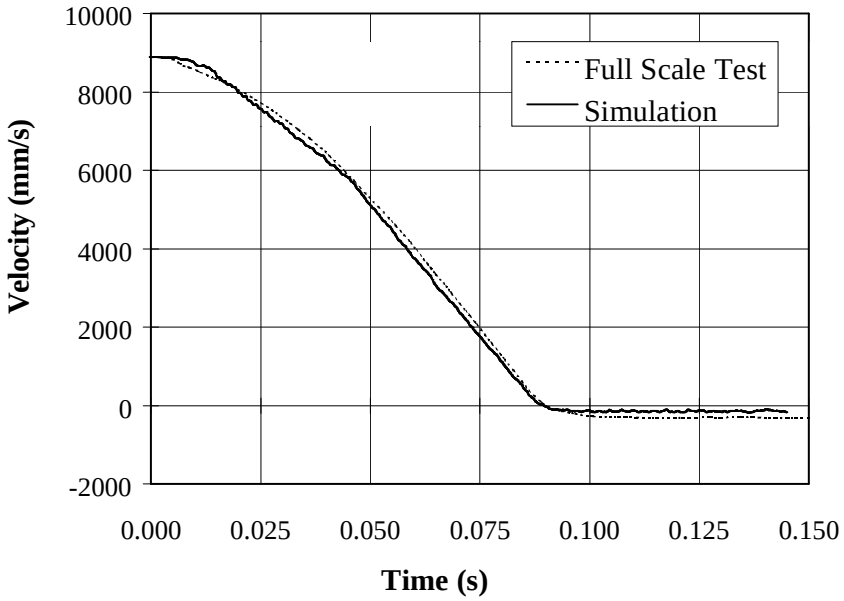

Figure 12. Comparison of velocity time histories from crash test and simulation of Bogie impacting a rigid pole at 32 km/hr. (20 mph)

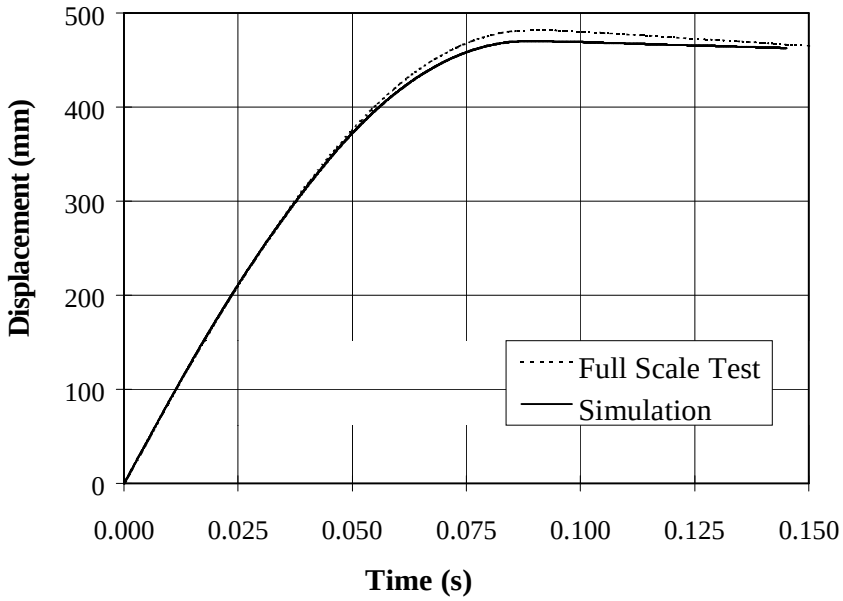

Figure 13. Comparison of displacement time histories from crash test and simulation of Bogie impacting a rigid pole at 32 km/hr. (20 mph)

ACKNOWLEDGMENT

This research is conducted at the FHWA/NHTSA National Crash Analysis Center (NCAC) with funding from the US Federal Highway Administration. The efforts of Mr. Ahmad Gaith of the NCAC for the preparation of Bogie's geometric data, drawings and laboratory testing, and the initial modelling and the assistance of FHWA's Federal Outdoor Impact Laboratory (FOIL) are greatly appreciated.

REFERENCES

1. W. Johnson, "Introduction to crashworthiness", *International Journal Of Crashworthiness,* (1996) Vol. 1, No. 1, pp. 5-10.
2. W. Johnson, "The elements of Crashworthiness: Scope and Actuality", *Proc. Inst. Mech. Engrs.*, (1990), 204, *Part D, J. of Automobile Eng.*, pp. 255-273.
3. "Occupant protection and Injury Assessment in the Automotive Crash Environment", *Proc. of SAE International Congress and Exposition, Detroit Michigan*, (1997), SP-123, pp. 35-107.
4. "Issues in automotive safety technology", *Proc. of SAE International Congress and Exposition, Detroit Michigan*, (1995), SP-1072, pp. 123-279.
5. T. Belytschko, "On Computational methods for Crashworthiness", Proceedings of the 7th International Conference on Vehicle Structural Mechanics, SAE, Detroit, (1988), pp. 93-102.
6. Fourth International LS-DYNA3D Conference, Minneapolis, Minnesota, USA, *Proceedings by Livermore Software Technology Corp., Livermore, CA.*, (1996), pp. 313-333.

7. D.J. Benson, *et. al.*, "The Application of DYNA3D in Large Scale Crashworthiness Calculations," *Proceeding of International Computers in Engineering Conference*, ASME, (1986), pp. 311-317.

8. R.G. Whirley, and B. Englemenn, "Automatic Contact in DYNA3D for Crashworthiness and impact problems', *J. of Nuclear Engineering and Design, Elsevier Science*, (1994), pp. 225-233.

9. R.G. Whirley, and B. Englemenn, "Automatic Contact in DYNA3D for Vehicle Crashworthiness', *Crashworthiness and Occupant Protection in Transportation Systems*, AMD-Vol. 169/BED-Vol. 25, ASME, (1993), pp. 15-29.

10. D. Marzougui, C.D. Kan, and N.E. Bedewi, "Development and Validation of an NCAP Simulation Using LS-DYNA3D", *Proc. Of Fourth International LS-DYNA3D Conference*, (1996), Minneapolis, Minnesota, pp. 319-332.

11. A.K. Zaouk, N.E. Bedewi, C.D. Kan, and H. Schinke, "Evaluation of a Multi-purpose Pick-up Truck Model Using Full Scale Crash Data with Application to Highway Barrier Impacts", *Proceedings of the 29th ISATA, Florence, Italy*, (1996), Paper No. 96SAF056, pp. 39-46.

12. N.E. Bedewi, T. Omar, and A. Eskandarian, "Effect of Mesh Density Variation in Vehicle Crashworthiness Finite Element Modeling", *Proceedings of ASME Winter Annual Meeting, DSC-Vol.54/DE-Vol.76, Transportation Systems Session*, (1994), Chicago, IL, pp. 495-504.

13. N.E. Bedewi, C.D. Kan, S. Summers, and C. Ragland, "Evaluation of Car-to-Car Frontal Offset Impact Finite Element Models Using Full Scale Crash Data", *Proc. of SAE International Congress and Exposition, Detroit Michigan*, (1995), SP-1072, 950650, pp. 211-219.

14. E.C. Chirwa, "Structural crashworthiness simulation of a rear-end collision of a small European car", *International Journal Of Crashworthiness*, (1996) Vol. 1, No. 1, pp. 21-34..

15. S. Varadappa, S.C. Shyo, and A. Mani, "Development of a passenger vehicle finite element model", *Final Report US DOT HS 808 145, US Department of Transportation*, (1993), Washington, D.C., pp. 34-52.

16. A. K. Zaouk, N.E. Bedewi, C.D. Kan, and D. Marzougui, "Development and Evaluation of A C-1500 Pickup Truck Model For Roadside Hardware Impact Simulation', *Proceedings of FHWA Vehicle Crash Analysis Conference*, Publication No. FHWA-RD-96-212, (1997), pp. 1-31.

17. A. Toyoma, K. Hatano, and E. Murakami "Numerical Analysis of Vehicle Frontal Crash Phenomena", *Analytical modeling and occupant protection technologies, SAE*, (1992), pp. 143-154.

18. T. Frank, and K. Gruber, "Numerical Simulation of Frontal Impact and front Offset Collisions," *Cray Channels*, (1991), pp. 2-6.

19. D. Schaur, et. al. "Preliminary Vehicle Impact Simulation Technology Advancement (Pre-Vista)", *Report, FHWA-RD-96-059*, Federal Highway Administration, Washington, D.C., (1997), pp. 55-118.

20. B.F. Hendricks, O. S. Martin, and J.W. Wekezer, "Impact Simulation of The 820C Vehicle with the G2 Guardrail," *Proceedings of FHWA Vehicle Crash Analysis Conference*, Publication No. FHWA-RD-96-212, (1997), pp. 129-147.

21. A. Eskandarian, N.E. Bedewi, and D. Marzougui, "Failure Analysis of Highway Small Sign Support Systems in Crashes Using Impact Finite Element Methods", *Proceedings of the 29th ISATA, Florence, Italy*, (1996), Paper No. 96SAF064, pp. 395-402.

22. A. Eskandarian, A. Gaith, D. Marzougui, and N.E. Bedewi, "Finite Element Impact Modeling of Slip Base Breakaway Sign Support Systems", presented at *Transportation Research Board Annual Meeting, Computer simulation of impact with roadside safety features*, (1995), pp. 1-50.

23. A. Eskandarian, N.E. Bedewi, and D. Marzougui, "Finite Element Modeling of Highway Narrow Objects", *presented at Transportation Research Board Annual Meeting, Computer simulation of impact with roadside safety features*, (1994), pp. 1-35.

24. J. W. Wekezer, M. Oskard, R. Logan, and E. Zywicz, "Vehicle Impact Simulation", *Journal of Transportation Engineering*, Vol. 119, (1993), pp. 598-617.

25. J.O. Hallquist, *LS-DYNA3D Theoretical Manual*, Livermore Software Technology Corporation, LSTC report 1018, Rev. 3, (1994).

26. J.O. Hallquist, D.W. Stillman, and T.L. Lin, *LS-DYNA3D Users Manual*, Livermore Software Technology Corporation, LSTC report 1007, Rev. 3, (1995).

27. R.G. Whirley, and J.O. Hallquist, "DYNA3D , a nonlinear, explicit, three-dimensional finite element code for solid and structural mechanics. User Manual", *Report No. UCRL-MA-107254, Lawrence Livermore National Laboratory*, May, (1991).

28. A. Malliaris, "Crash and Casualty Characterization of Light Vehicle Side Impacts with Narrow objects" FHWA/NHTSA National Crash Analysis Center Report, (1994), pp.-50.

29. H.E. Junior Ross, D.L. Siking, R.A. Zimmer, and J.D. Michie, "Recommended Procedures for the Safety Performance Evaluation of Highway Appurtenances", *Transportation Research Board, National Research Council, National Cooperative Highway Research Program*, Report 350, (1993), pp. 1-64.

30. J. Hinch, G. Manhard, D. Stout, R. Owings, "FOIL Construction, Laboratory Procedures to Determine The Breakaway Behavior of Luminare Supports in Mini-sized Vehicle Collisions", Vol. I, II, and III. *FHWA Report Nos*. FHWA/RD-86/105, 106, and 107, Wash. D.C., (1987).

31. C. Hott, C. Brown, N. Totani, and A. Hansen, "Validation of a Surrogate Vehicle for Certification Testing of Transformer Base Luminare Supports", *Federal Highway Administration, Report No.* FHWA/RD-87/034, (1988), pp. 1-98.

32. C. Hott, C. Brown, N. Totani, and A. Hansen, "Crush Characteristics of the Breakaway Bogie", *Federal Highway Administration, Report No.* FHWA/RD-89/107, (1990), 1-75.

33. "Mechanical Properties of Hexcel Honeycomb Materials", *Hexcel Corporation, Dublin, CA., USA,* Report No. Revised TSB 120, (1966).

34. L. E. Schwer, and R.G. Whirley, "Lessons Learned in modeling a moving deformable barrier (MDB) impacting a rigid wall", *International Journal Of Crashworthiness,* Woodhead Publ., (1996), Vol. 1, No. 1, pp. 73-92.

35. J. Hinch, R. Owings, and G. Manhard, "Development Testing For Foil Bogie Test Results Report", Task D, *Federal Highway Administration Contract No. DTFH61-89-C-00036* (1985), pp. 1-54.